Darcy Forchheimer flow of CMC-water based hybrid nanofluid due to a rotating stretchable disk

Farhan Ali [a], Muhammad Arif [b], Muhammad Faizan [a], Anwar Saeed [b], Thidaporn Seangwattana [c,*], Poom Kumam [b,d,**], Ahmed M. Galal [e,f]

[a] *Department of Mathematical Sciences, Federal Urdu University of Arts, Sciences & Technology, Gulshan-e-Iqbal Karachi, 75300, Pakistan*
[b] *Center of Excellence in Theoretical and Computational Science (TaCS-CoE), King Mongkut's University of Technology Thonburi (KMUTT), 126 PrachaUthit Rd., Bang Mod, ThungKhru, Bangkok, 10140, Thailand*
[c] *King Mongkut's University of Technology North Bangkok, Rayong Campus (KMUTNB), 21120, Rayong, Thailand*
[d] *Department of Medical Research, China Medical University Hospital, China Medical University, Taichung, 40402, Taiwan*
[e] *Department of Mechanical Engineering, College of Engineering in WadiAlddawasir, Prince Sattam bin Abdulaziz University, Saudi Arabia*
[f] *Production Engineering and Mechanical Design Department, Mansoura University, P.O 35516, Mansoura, Egypt*

ARTICLE INFO

ABSTRACT

The flow of fluid over a spinning disk has a broad scope of numerous applications. It is employed in various things, including medical equipment, the braking system of cars, gas turbines, plastic films, and glass production. As a result of these applications, we considered the phenomena of Darcy Forchheimer's three-dimensional flow on $TiO_2 - Fe_3O_4$ nanoparticles suspended in based CMC-water fluid. The influence of thermal radiation and convective conditions is studied. Moreover, the Buongiorno model is utilized to compute the Brownian motion and the thermophoretic effect. To generate the non-dimensionalized governing equations, suitable alterations are put into use. These equations are then utilized with Matlab BVP4c. Graphs are used to analyze the behavior of velocity distributions, and thermal and concentration profiles at different parameter values. In addition, the solutions to the flow problem have been analyzed in terms of several other physical variables on velocity, temperature, concentration, drag force, heat, and mass transfer. According to the findings, it is clear that an escalates in the value of the rotation parameter leads to an increase in the radial velocity and axial velocity. In contrast, an opposite pattern is followed in the Forchheimer number. Finally, some engineering quantities are evaluated numerically and presented in tabular forms.

1. Introduction

Adequate drilling fluid, often known as drilling mud, is necessary for a successful drilling operation. The high viscosity of cellulose derivative carboxymethyl cellulose (CMC) makes it a popular substance. However, its low heat conductivity limits its usefulness as a drilling fluid in extreme conditions. The fluid's efficiency is improved when nanoparticles are dispersed throughout CMC in a colloidal mixture. Mondal [1] recently addressed the characteristics, features, and synthesis of CMC aqueous solution. It has high solubility

potential, and the capability to soak up and hold water, control the growth of crystals, enhance shelf life, and give the desired texture to the body. They keep in mind these unique properties and the multifunctional aspects of CMC in various industrial and technological applications. Benchabane and Bekkour [2] inspected the impact of moisturization due to the CMC polymeric structure, which has practical applications in the film-forming factor. After this, Babazadeh et al. [3] the authors inspected some practical applications of CMC fluids in the pharmaceutical and paper industries. Siqueira et al. [4] studied CMC as a model compound used in paper industries. Ali et al. [5]described the entropy generation for Cross hybrid water-based CMC solution. The impact of CMC in heat and mass transfer applications and many other industrial and engineering applications of CMC are found in Refs. [6–9].

Researchers have been interested in the efficacy of liquids as a subject of study because of industrial applications that include heat transmission. Conventional liquids such as ethylene glycol, water, and oil are utilized in various machinery and equipment; however, these liquids have a narrower range of temperatures. Various investigators have attempted to boost the thermophysical features of liquids and reduce the thermal expansion challenges by inserting a few solid nanosized particles into the liquid. It has been done to strengthen the thermal physical characteristics of liquids. In their initial conversation, Choi and Eastman [10] talked about the thermophysical features of nanofluid. A new type of nanofluid has been developed to provide the industry with the maximum heat transfer required. This nanofluid consists of two or more different nanoparticles suspended in a base liquid. This sort of nanofluid, known as a hybrid nanofluid, operates at temperatures significantly more significantly compared to nanofluid. Similar studies on nanofluids have been conducted by numerous scientists [11–21]. The transport phenomenon of nanofluids was first described by Buongiorno [22] in the year 2006; it is a model that is superior to dispersion and homogeneous models in that it incorporates the nature and properties of nanoparticles as well as those of the carrier liquid. This model has been hailed as an improvement. Abbasi et al. [23] examined the slip effect on hybrid nanoparticles over a wave surface. Chu et al. [24] probed the numerical investigation of a hybrid nanofluid using different nanoparticles via various heat sources. Ullah et al. [25] accomplished thermal radiative with water base hybrid nanofluid due to a spinning disk. Sowmya et al. [26] studied the combined effect of heat generation and convective conditions for a hybrid nanofluid due to a porous fin. Xue et al. [27] pondered the mixed convective hybrid nanofluid inside a microchannel. Laiquat et al. [28] endeavored the boundary layer flow of shrinking surface and hybrid nanoparticles past a spongy surface. Lately, Hassan et al. [29] suggested the MHD flow of nonlinear thermal radiation of hybrid nanoparticles using CNTs due to a revolving disk. Nayak et al. [30] probed a combined effect of viscous dissipation and thermal radiation on MHD flow over a shrinking surface. Sadeghi et al. [31] reported a theoretical analysis of buoyancy-driven flow inside the two circular cylinders. Saw et al. [32] offered the thermal investigation of Cross hybrid nanofluid under quadratic radiative. Nayak et al. [33] explored the wavy Baffles for the implications of heat with dual diffusion natural convection flow. Sarangi et al. [34] discovered the impact of low and higher Prandtl numbers on tri-hybrid nanoliquid. Rout et al. [35] explored the second law analysis on Ferro-nanofluid with slip effect due to shrinking disk. Hakeem et al. [36] examined the MHD Carreau hybrid nanoparticles due to an exponential surface. Sharma et al. [37] reported the significance of the viscous dissipation of copper nanoparticles due to spinning disks. Kumar and co-worker [38] scrutinized the Darcy-Forchheimer flow and heat source/sink with a hybrid nanofluid. Kumar and co-worker [39] studied the entropy production of hybrid nanofluid above their revolving disk induced by partial slip.

Modern research fluids containing metallic and metal oxide nanoparticles have widely used applications in various physical situations. The metal oxide nanoparticles ZnO, Au, Fe_2O_3, and TiO_2 have been used in various physical problems to improve thermal transport properties. Recently, many scholars explored the impact of TiO_2 nanoparticles in different physical situations. Zental et al. [40] inspected TiO_2 nanoparticles and their medical applications. Then, Behnam et al. [41] explored how TiO_2 nanoparticles can be used in photo-thermal therapy and melanoma cancer model applications. After this, Shi et al. [42] examined the impact of titanium dioxide nanoparticles in different biological systems. Finally, some advanced physical applications of titanium dioxide nanoparticles have been used, which are mentioned in references [43–45].

To examine the flow of nanofluids and hybrid nanofluids, several studies were conducted on discs that ranged in shape, size, and material composition. Computers Disk and gas turbine power plants are only two examples of the many different types of mechanical equipment demonstrating the significance of rotation in heat transfer. Because of the rotating flow configuration, there are essential uses in frills, aviation engines, compressors engines, and propeller pumps. Flow also plays a role in some other industries. In addition to their use in engineering, microclimate systems, and electrochemistry, gyrating discs also have different applications. Karman [46] was the first researcher to investigate the flow across discs. Benton [47] explained the occurrence due to a rotating disk. Emslie et al. [48] inspected the viscous fluid flow over a rotating disk and its impact in different conditions. After this, Cobb and Saunders [49] where the authors discussed heat transfer features of rotating disks for various physical situations. Recently, many researchers examined the modern applications of the rotating disk in different physical conditions, Wang and a co-worker [50] studied the coupling of rotating disk electrodes for advanced applications in chemical processes and electrochemistry. Beg et al. [51] examined the numerical study of bioconvection nanofluid flow due to a rotary disk in a spongy surface with a slip effect. Gregory et al. [52] scrutinized the impact of stability analysis of the three-dimensional boundary layers with advanced applications to the flow due to the rotating disk. Mushtaq and Mustafa [53] deliberated on the examination of the nanofluid flow toward a stretched rotating disk in the presence of an axial magnetic field and convective conditions. Khan et al. [54] explored how MHD effect the nanofluid flow and heat transfer analysis due to a revolving disk. Asma et al. [55] inspected the numerical investigations of the Darcy-Forchheimer flow above a revolving disk with the applications of nanoparticles in the heat transfer rate. Rehman et al. [56] calculated the numerical analysis of Casson fluid flow over a rigidly revolving disk with the MHD effect. Some other studies of turning disk flow and its physical applications are addressed in references [57–60].

- Motivated by the literature mentioned above survey, to the best of the author's knowledge, no analysis is recorded to explore a numerical analysis of Darcy Forchheimers flow of CMC-water-based hybrid nanofluid past a rotating stretchable disk.

- The primary idea of this study is to improve our perception of the exhaustion of energy in industrial and engineering fields. In addition, water is selected as a base fluid, and two different nanoparticles are tested and compared for their thermal efficiency on the water-based fluid flow over a rotating disk.
- The obtained system of high nonlinear equations is handled numerically by employing the bvp4c numerical scheme.
- The impact of velocities, temperatures, and concentrations graphs have been drawn to discuss the effects of many influential parameters.
- The primary outcomes of the present research focused thermal performance of Fe_3O_4 and TiO_2 nanoparticles on the water-based fluid and their comparison is presented in all graphs.
- In addition, Calculations and inspections are performed on the numerical values of skin frictions as well as local Sherwood and Nusselt numbers. Moreover, the data presented here perfectly accord with the tabulated findings of an earlier published study.

2. Mathematical modeling

Consider the steady incompressible Darcy Forchheimers flow of CMC-water hybrid nanofluid to a rotating stretchable disk. The current flow study has decided on a cylindrical coordinate system (r, φ, z). We assume that magnetite-CMC-water nanofluid flow over a rotating disk lying $z = 0$ plane. In the base fluid, water Fe_3O_4 and TiO_2 nanocomposites are dispersed for thermal transport applications. The Buongiorno model is applied. The thermal characteristics properties of water base fluid containing Fe_3O_4 nanoparticles are compared with the water having TiO_2 nanoparticles. The motion in the liquid is produced over the rigid body rotation of the disk in a positive φ direction with constant angular acceleration ω (see Fig. 1).

Moreover, the wall temperature is denoted by T_w and the ambient temperature T_∞ from the flow geometry, so the temperature difference is noticed $T_w > T_w$. Finally, due to the problem's axial symmetry, the derivative w.r.t coordinate φ is ignored. Using the above assumptions, the governing equations of the present proposed model can be expressed as follows [50,51]:

$$\frac{\partial u}{\partial r} + \frac{u}{r} + \frac{\partial w}{\partial z} = 0 \tag{1}$$

$$u\left(\frac{\partial u}{\partial r}\right) - \frac{v^2}{r} + w\left(\frac{\partial u}{\partial z}\right) = \frac{\mu_{hnf}}{\rho_{hnf}}\left(\frac{\partial^2 u}{\partial z^2} + \frac{1}{r}\frac{\partial u}{\partial r} - \frac{u}{r^2} + \frac{\partial^2 u}{\partial r^2}\right) - \frac{v_{nf}}{K^*}u - Fu^2 \tag{2}$$

$$u\left(\frac{\partial v}{\partial r}\right) + \frac{uv}{r} + w\left(\frac{\partial v}{\partial z}\right) = \frac{\mu_{hnf}}{\rho_{hnf}}\left(\frac{\partial^2 v}{\partial z^2} + \frac{1}{r}\frac{\partial v}{\partial r} - \frac{v}{r^2} + \frac{\partial^2 v}{\partial r^2}\right) - \frac{v_{nf}}{K^*}v - Fv^2 \tag{3}$$

$$u\left(\frac{\partial T}{\partial r}\right) + w\left(\frac{\partial T}{\partial z}\right) = \frac{\ell_{hnf}}{(\rho C_p)_{hnf}}\left(\frac{\partial^2 T}{\partial r^2} + \frac{1}{r}\frac{\partial T}{\partial r} + \frac{\partial^2 T}{\partial z^2}\right) + \tau\left[D_B\left(\frac{\partial T}{\partial z}\frac{\partial \mathscr{C}}{\partial z} + \frac{\partial T}{\partial r}\frac{\partial \mathscr{C}}{\partial r}\right) + \frac{D_T}{T_\infty}\left[\left(\frac{\partial T}{\partial z}\right)^2 + \left(\frac{\partial T}{\partial r}\right)^2\right]\right] \tag{4}$$

$$u\left(\frac{\partial \mathscr{C}}{\partial r}\right) + w\left(\frac{\partial \mathscr{C}}{\partial z}\right) = D_B\left(\frac{\partial^2 \mathscr{C}}{\partial z^2} + \frac{1}{r}\frac{\partial \mathscr{C}}{\partial r} + \frac{\partial^2 \mathscr{C}}{\partial r^2}\right) + \frac{D_T}{T_\infty}\left(\frac{\partial^2 T}{\partial r^2} + \frac{1}{r}\frac{\partial T}{\partial r} + \frac{\partial^2 T}{\partial z^2}\right) \tag{5}$$

Boundary conditions is defined as [6]

$$\left.\begin{array}{l} u = cr, v = \omega r, w = 0, -k_{hnf} = h_f\left(T_f - T\right), C = C_w, z \to 0 \\ u \to 0, v \to 0, T = T_\infty, C = C_\infty, z \to \infty \end{array}\right\} \tag{6}$$

where components u, v, and w are velocity components in r, φ, z direction, respectively. The fluid temperature is represented by T, C stands for nanoparticle concentration, μ_{hnf} denotes the dynamics viscosity, ρ_{hnf} shows the density, ℓ_{hnf} shows thermal conductivity, $(\rho C_p)_{hnf}$ shows the heat capacitance of the hybrid nanofluid, D_B stands for Brownian diffusion coefficient, D_T for thermophoretic diffusion coefficient.
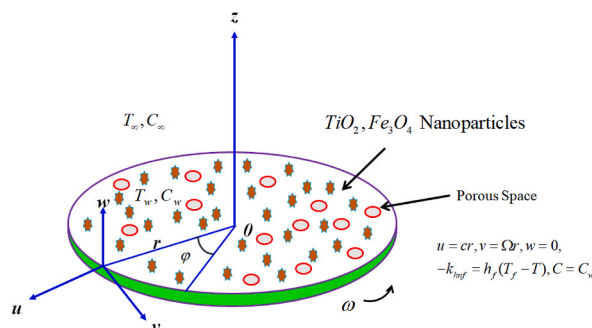
Fig. 1. Flow geometry.

$$\frac{\mu_{hnf}}{\mu_f} = \frac{1}{(1-\varphi_1)^{2.5}(1-\varphi_2)^{2.5}}$$

$$\frac{\rho_{hnf}}{\rho_f} = (1-\varphi_2)\left[(1-\varphi_1)+\frac{\varphi_1\rho_{1s}}{\rho_f}\right]+\frac{\varphi_2\rho_{2s}}{\rho_f}$$

$$\frac{k_{hnf}}{k_f} = \frac{k_{2s}+2k_f-2\varphi_2(k_f-k_{2s})}{k_{2s}+2k_f+\varphi_2(k_f-k_{2s})}\times k_{nf}$$

$$\frac{k_{1s}+2k_f-2\varphi_1(k_f-k_{1s})}{k_{1s}+2k_f+\varphi_1(k_f-k_{1s})}$$

$$\frac{(\rho\,C_P)_{hnf}}{(\rho\,C_P)_f} = (1-\varphi_2)\left[(1-\varphi_1)+\frac{\varphi_2(\rho C_P)_{1s}}{(\rho C_P)_f}\right]+\varphi_2\left(\frac{(\rho C_P)_{2s}}{(\rho C_P)_f}\right)$$

(7)

In Eq. (7), the mathematical expression φ_1 and φ_2 represent the volume fraction of solid nanoparticles of the TiO_2 and e_3O_4, respectively. Further, the subscripts $f, hnf, 1s,$ and $2s$ exhibit the base fluid, hybrid nanoparticles, and the two distinct solid nanofluids. The physical data of these hybrid nanoparticles. Thermophysical characteristics of TiO_2 and Fe_3O_4 with CMC-water base fluid are displayed in Table 1.

The variables transformation is described as [61]

$$u = cr, v = \omega r, w = 0, -k_{hnf}\left(\frac{\partial T}{\partial z}\right) = h_f(T_f-T), C = \mathscr{C}_w \; at \; z = 0$$

$$u{\rightarrow}0, v{\rightarrow}v_e = 0, T{\rightarrow}T_\infty, \mathscr{C}{\rightarrow}\mathscr{C}_\infty \; at \; z = \infty$$

(8)

$$.$$

The following transformation are [61]

$$u = c\,rF(\eta), v = c\,rG(\eta), w = \sqrt{c\,\vartheta_f}H(\eta),$$

$$\eta = \sqrt{\frac{c}{\vartheta_f}}\,z, \theta(\eta) = \frac{T-T_\infty}{T_W-T_\infty}, \psi(\eta) = \frac{\mathscr{C}-\mathscr{C}_\infty}{\mathscr{C}_\infty}\;.$$

(9)

Applying the considered similarity variables on Eqs. (1)–(5), the transform system of governing equations are given as follows [61]

$$2F+H^{'} = 0 \tag{10}$$

$$F^{''}+\left(\frac{A_2}{A_1}\right)\left[G^2-F^2-H\,F^{'}-\lambda F\right]-FrF^2 = 0 \tag{11}$$

$$G^{''}+\left(\frac{A_2}{A_1}\right)[2\,F\,G+H\,G^{'}-\lambda G]-FrG^2 = 0 \tag{12}$$

$$\theta^{''}+\left(\frac{Pr}{A_3}\right)\left[Nb\,\theta^{'}\psi^{'}+Nt\,(\theta^{'})^2-A_4\,H\,\theta^{'}\right] \tag{13}$$

$$\psi^{''}+\left(\frac{Nt}{Nb}\right)\theta^{''}-Sc\,H\,\psi^{'} = 0 \tag{14}$$

In which,

Dynamic viscosity $= A_1 = \frac{\mu_{hnf}}{\mu_f}$, Density $= A_2 = \frac{\rho_{hnf}}{\rho_f}$, Thermal conductivity $= A_3 = \frac{k_{hnf}}{k_f}$, heat capacity $= A_4 = \frac{(\rho C_P)_{hnf}}{(\rho C_P)_f}$.

Here, the altered conditions are:

$$F(0) = 1, G(0) = \beta, H(0) = 0, \theta^{'}(0) = -A_4 Bi(1-\theta(0)), \psi(0) = 1$$

$$F(\infty){\rightarrow}0, G(\infty){\rightarrow}0, \theta(\infty){\rightarrow}0, \psi(\infty){\rightarrow}0$$

(15)

where during performing the similarity transformation we get the following dimensionless parameters $M, \lambda, Fr, Nt, Nb, Pr, Sc, \beta, and\, Re$

Table 1
Thermophysical properties of water base fluid TiO_2 and Fe_3O_4 nanoparticles are given as.

Physical properties	Specific heat capacity	Density	Thermal conductivity
CMC-water ($<0.4\%$)	4179	997.1	0.613
TiO_2	686.2	4350	8.95
Fe_3O_4	670	5180	9.7

are magnetic field, porosity parameter, Forchheimer number, Thermophoresis parameter, Brownian motion, Prandtl number, Schmidt number, rotational parameter.

$$M = \frac{\sigma_f B_0^2}{\rho_f \text{c}}, \lambda = \frac{v}{\text{k} * \Omega}, Fr = \frac{Cb}{k^{\frac{1}{2}}}, Nt = \frac{\tau D_T (\text{T}_W - T_\infty)}{T_\infty \vartheta_f}$$

$$Nb = \frac{\tau D_B (\mathscr{C}_\infty)}{\vartheta_f}, Pr = \frac{(\mu C_P)_f}{\kappa_f}, Sc = \frac{\vartheta_f}{D_B}, \beta = \frac{\omega}{\text{c}}.$$

Physical Quantities: Physical quantities of the present model is expressed as [50,51]:

$$C_f = \frac{\sqrt{\tau_r^2 + \tau_\theta^2}}{\rho_f (cr)^2}, Nu = \frac{r q_w}{\mathscr{l}_f (T_W - T_\infty)}, Sh = \frac{r j_w}{D_f (C_W - C_\infty)} \Biggr\} \tag{16}$$

Here, τ_r and τ_θ is described as radial and transverse stress, q_w and j_w represented by heat and mass flux [50,51]

$$\tau_r = \left[\mu_{nf} \left(\frac{\partial u}{\partial z} + \frac{\partial w}{\partial \varphi} \right) \right]_{z=0}, \tau_\theta = \left[\mu_{nf} \left(\frac{\partial v}{\partial z} + \frac{1}{r} \frac{\partial w}{\partial \varphi} \right) \right]_{z=0} \Biggr\} \tag{17}$$

$$q_w = -\frac{\mathscr{l}_{nf}}{\mathscr{l}_f} \left(\frac{\partial T}{\partial z} \right)_{z=0}, j_w = - \left(\frac{\partial C}{\partial z} \right)_{z=0},$$

The reduced form of friction force, heat and mass are described as [50,51].

$$C_f Re^{\frac{1}{2}} = A_1 \sqrt{(F'(0))^2 + (G'(0))^2}, NuRe^{-\frac{1}{2}} = -A_3 \theta'(0), ShRe^{-\frac{1}{2}} = -\psi'(0) \Biggr\} \tag{18}$$

3. Solution strategy

The numerical code bvp4c is created to study the flow model, which is explained by Eqs.(11)–(14) with the associated boundary conditions. Eq. (15) is also altered according to first-order ODEs. Due to their nonlinear nature, these equations make it challenging to find an accurate solution to the issues they describe. There are several ways to work with numbers that use arbitrary parameters or discretizations. Such plans are hard to carry out. The Runge–Kutta method is easy to understand, saves money, and is accessible to code. The process guarantees a rapid and consistent convergence even with significant volatility in the parameters that regulate the system. Therefore, for this procedure, we assign a new variable [48,61].

$$\left. \begin{array}{l} F = R_1, \dfrac{dF}{d\xi} = R_2, \dfrac{d^2 F}{d\xi^2} = \dfrac{dR_2}{d\xi} \\[2mm] G = R_3, \dfrac{dG}{d\xi} = R_4, \dfrac{d^2 G}{d\xi^2} = \dfrac{dR_4}{d\xi}, H = R_5 \\[2mm] \theta = R_6, \dfrac{d\theta}{d\xi} = R_7, \dfrac{d^2 \theta}{d\xi^2} = \dfrac{dR_7}{d\xi} \\[2mm] \psi = R_8, \dfrac{d\psi}{d\xi} = R_9, \dfrac{d^2 \psi}{d\xi^2} = \dfrac{dR_9}{d\xi} \end{array} \right\} \tag{19}$$

The system of first-order differential equations becomes [48,61]

$$\left. \begin{array}{l} \dfrac{dR_2}{d\xi} = -\left(\dfrac{A_2}{A_1} \right) \left[R_3^2 - R_1^2 - R_2 R_5 - \varepsilon R_1 \right] + Fr R_1^2 \\[3mm] \dfrac{dR_4}{d\xi} = -\left(\dfrac{A_2}{A_1} \right) \left[2R_1 R_3 + R_4 R_5 + \varepsilon R_3 \right] + Fr R_3^2 \\[3mm] \dfrac{dR_5}{d\xi} = -2 \dfrac{dR_1}{d\xi} \\[3mm] \dfrac{dR_9}{d\xi} = -\left(\dfrac{Pr}{A_3} \right) \left[Nb R_7 R_8 + Nt R_7^2 - A_4 R_5 R_7 \right] \\[3mm] \dfrac{dR_9}{d\xi} = -\left(\dfrac{Nt}{Nb} \right) R_7' + Sc R_5 R_9 \end{array} \right\} \tag{20}$$

Transmuted boundary conditions are [48,61]

$$\left. \begin{array}{l} R_1(0) = 1, R_3(0) = \beta, R_5(0) = 0, R_7(0)(0) = -Bi(1 - R_8(0)), R_9(0) = 1 \\ R_1(\infty) \to 0, R_3(\infty) \to 0, R_6(\infty) \to 0, R_8(\infty) \to 0 \end{array} \right\} \tag{21}$$

The relative error tolerance has been set to 10-6.

4. Results and discussion

This section explored the graphical representation of the flow, heat, and concentration profiles against various involved parameters. The flow parameter of interest is Brownian motion *Nb*, thermophoresis parameter *Nt*, Prandtl number *Pr*, magnetic parameter *M*, volume friction parameter φ, rotation parameter β, and the local inertial factor *Fr*. In this analysis, we focused on exploring the impact of pertinent parameters on the axial velocity $F(\eta)$, radial velocity $G(\eta)$, azimuthal velocity $H(\eta)$, temperature $\theta(\eta)$, and concentration $\psi(\eta)$. In addition, some flow parameters are elucidated through trapping phenomenon and highlighted inthe figures. Moreover, numerical values of the Sherwood numberNusselt number and skin friction are evaluated and presented in tables for different pertinent flow parameters.

4.1. Impact of Darcy-Forchheimer Fr

The fluctuations of *Fr* versus axial velocity $F(\eta)$, radial velocity $G(\eta)$, azimuthal velocity $H(\eta)$ and temperature $\theta(\eta)$ for the $TiO_2 + CMC - water$ and $Fe_3O_4 + CMC - water$ based nanofluid are highlighted in Fig. 2(A)–(D), respectively. It is worth noting here in the present analysis. We have compared the water-based nanofluid containing TiO_2 and Fe_3O_4 nanoparticles in all the radial, axial and azimuthal velocities, along with the heat and concentration of the fluid. In the present article, fascinating results were obtained during the analysis of *Fr* flow profiles along with heat profiles with the comparative study between the TiO_2 and Fe_3O_4 nanoparticles in the base fluid water. The impact of escalating values *Fr* on the axial and radial velocity are highlighted in Fig. 2(A) and (B), respectively. From both figures, the magnitude of the velocity gradient declines for the elevated values of *Fr* on the axial and radial velocity profiles. During the analysis, it was found that boosting amplitude of *Fr* developed some extra resistive forces within the fluid during the dynamics of the liquid over a rotating disk. Therefore, these resistive forces are generated due to the boosting values of *Fr*, and the axial and radial velocities decelerate due to the magnitude of the velocity distribution for the positive values *Fr*. The impact *Fr* on the azimuthal velocity profile is highlighted in Fig. 2(C). From the figure, the higher the importance of the *Fr* azimuthal velocity profile increase, as shown in the figure. The fascinating result was obtained during the analysis of *Fr* over the temperature of the fluid. The impact of *Fr* on $\theta(\eta)$ is highlighted in explored in Fig. 2(D). From the figure, elevated values *Fr* make an increase in the temperature
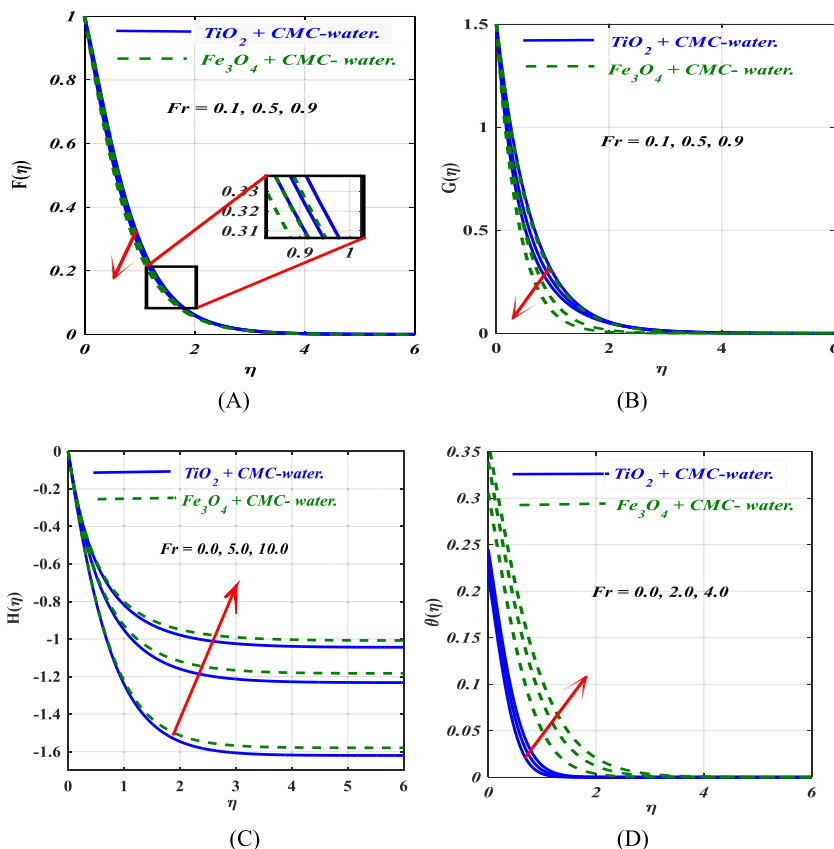
Fig. 2. Consequence of *Fr* on $(A)F(\eta)(B)G(\eta)(C)H(\eta)(D)\psi(\eta)$.

profile $\theta(\eta)$, as shown in the figure.

4.2. Impact of rotational parameter β

The increment of the rotational parameter β, and its impacts on the axial velocity $F(\eta)$, radial velocity $G(\eta)$, azimuthal velocity $H(\eta)$ profiles are highlighted. The fluctuations of β versus velocity $F(\eta)$, radial velocity $G(\eta)$, and azimuthal velocity $H(\eta)$ for the TiO_2+ $CMC - water$ and $Fe_3O_4 + CMC - water$ based nanofluid are elucidated in Fig. 3(A)–(C) respectively. Fig. 3(A) shows how β affects radial velocity. Increasing β increases radial velocity β grows as the disk rotates. Centrifugal force pulls fluid particles radially. Fig. 3(B) shows how rotational parameter β affects boundary layer tangential velocity. The rotation parameter improves tangential velocity distribution. Physically, disk rotation increases tangential velocity. We found that β has a greater influence on the disk surface than at the boundary layer edge. Fig. 3(C) shows how increasing the rotation parameter increases the fluid's negative z direction. The disk's rotation forces additional fluid to the surface, reducing azimuthal velocity.

4.3. Impact of volume fraction φ

The fluctuations of φ versus velocity $F(\eta)$, radial velocity $G(\eta)$, azimuthal velocity $H(\eta)$ and temperature $\theta(\eta)$, for the $TiO_2+ CMC-$ $water$ and $Fe_3O_4 + CMC - water$ based nanofluid are highlighted in Fig. 4(A)–(D) respectively. During the analysis, we judge the impact of different volume friction φ on the velocities and temperature of the fluid containing nanoparticles. In addition, we have two different nanoparticles and their thermal characteristics on the performance of the water-based fluid. It can be observed that in all the figures, we highlights the impact of volume friction in the case of TiO_2 and Fe_3O_4 nanoparticles in the base fluid water and found its behavior during the fluid flow dynamics over a stretching rotating disk. In this research, we obtained some excellent thermal characteristics of the suspended nanoparticles on the heat transfer rate. The impact of elevated values of φ on the axial and radial velocity are highlighted in Fig. 4(A) and (B), respectively. From both figures, the magnitude of the velocity gradient declines for the elevated values of φ on axial and radial velocity profiles. During the analysis, it was found that the boosting values of φ increased the concentration of the fluid, due to which the internal viscous forces within the fluid get higher, which produces extra resistive forces. As a result, fluid velocities decline in both axial and radial velocities. Furthermore, the boosting values of φ in both the cases TiO_2 and Fe_3O_4 nanoparticles suspended in the water have the same effect on the fluid flow over a rotating disk. The impact φ on the azimuthal velocity profile is highlighted in Fig. 4(C). From the figure the higher the values of the φ azimuthal velocity profile increase as shown in the figure. An excellent thermal characteristic is noticed during the analysis of φ on the temperature of the fluid. The impact of φ on $\theta(\eta)$, is
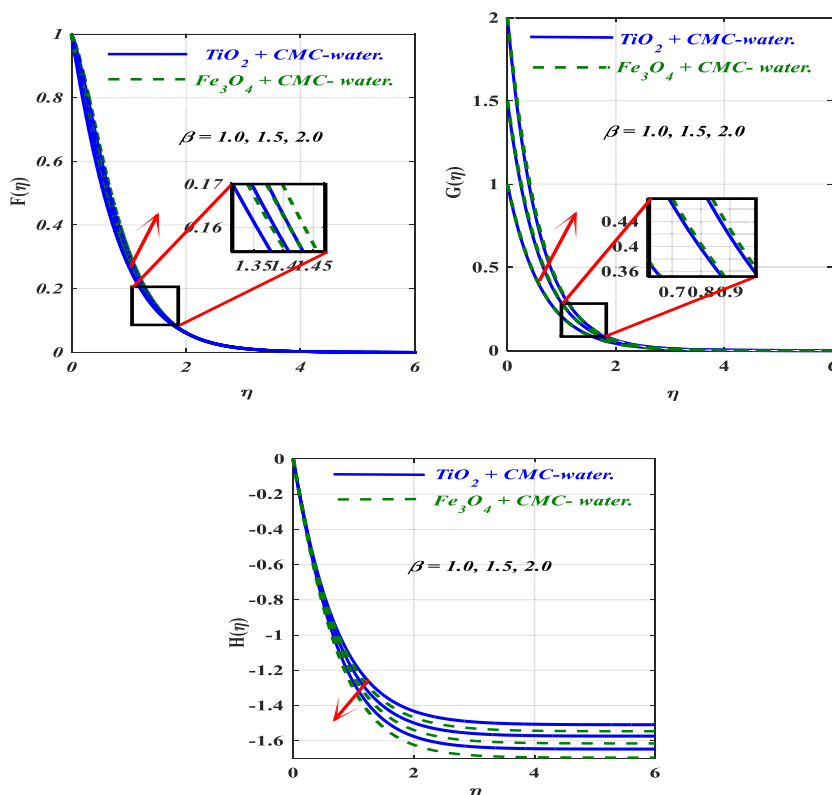
Fig. 3. Consequence of β on $(A)F(\eta)(B)G(\eta)(C)H(\eta)$.
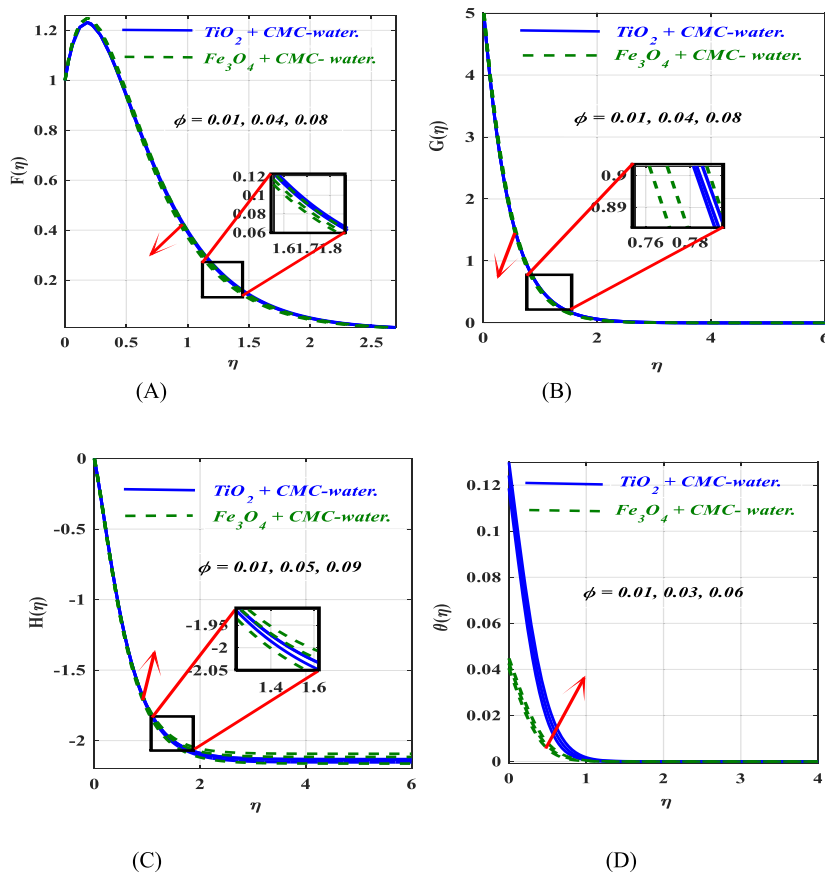
Fig. 4. Consequence of φ on $(A)F(\eta)(B)G(\eta)(C)H(\eta)(D)\theta(\eta)$.

highlighted and explored in Fig. 4(D). From the figure, elevated values of φ make an increase in the $\theta(\eta)$, as shown in the Figure. This increase in temperature occurs due to the rise in nanoparticle concentrations in the fluid. As the concertation of nanoparticles increases in the nanofluid with the higher values of φ in both the cases TiO_2 and Fe_3O_4 nanoparticles due to this increase in the concentration, a friction force developed in the fluid particles, which enhances the temperature of the fluid, as shown in Fig. 4(D).

4.4. Impact of thermophoresis parameter Nt

The fluctuations of Nt versus temperature $\theta(\eta)$ and concentration $\psi(\eta)$ for the $TiO_2 + CMC - water$ and $Fe_3O_4 + CMC - water$ nanofluid is highlighted in Fig. 5(A) and (B) respectively. The impact of various values of the thermophoretic parameter Nt on $TiO_2 +$
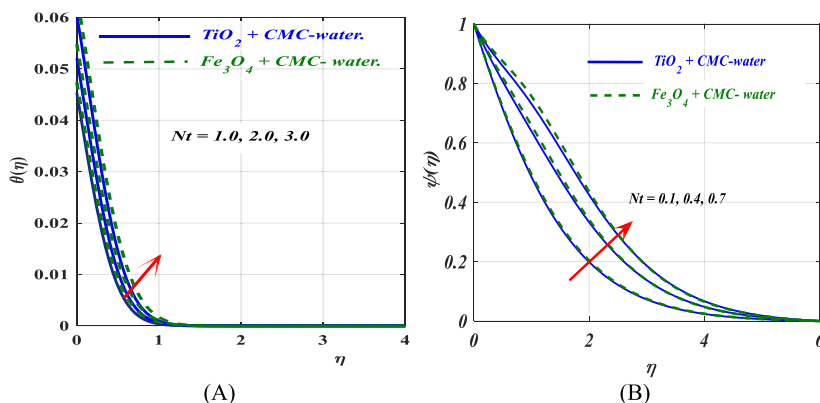
Fig. 5. Consequence of Nt on $(A)\theta(\eta)(B)\psi(\eta)$.

$CMC - water$ and $Fe_3O_4 + CMC - water$ nanofluid on thermal distribution is portrayed in Fig. 5(A). From the figure, the increase in temperature curves due to the escalating values of Nt is noticeable physically. The rise in Nt speeds up the thermophoretic process. The thermophoresis phenomenon occurs in the form of molecular mobility occurs when the temperature gradient is imposed. By imposing the thermal gradient, the uniform distribution of particles like $TiO_2 + CMC - water$ and $Fe_3O_4 + CMC - water$ basenanofluid flow over a stretching rotating disk transmits thermal energy very rapidly within the thermal boundary lyre region from the hotter surface to the cooler part. As a result, the temperature of the fluid gets high as shown in Fig. 5(A). Similarly, the nanoparticle concentration profile $\psi(\eta)$ for the escalating values of Nt on the $TiO_2 + CMC - water$ and $Fe_3O_4 + CMC - water$ base nanofluid is portrayed in Fig. 5(B). The plot of the higher value Nt versus concertation profiles $\psi(\eta)$ shows an increment behavior, it has been observed during the dynamics of nanofluid flow over a stretching rotating disk through the process Nt and is used as a supporting factor for the increases in the fluid concentration within the boundary, and physically it is correct. These obtained results highlight that Nt is used to develop the thermophoretic process, due to which the concentration gets higher, as shown in the figure.

4.5. Impact of Brownian motion parameter Nb

The variations of Nb versus temperature $\theta(\eta)$ and concentration $\psi(\eta)$ for the $TiO_2 + CMC - water$ and $Fe_3O_4 + CMC - water$ nanofluid are highlighted in Fig. 6(A) and (B) respectively. The temperature curve for various values of Nb the parameter is highlighted in Fig. 6(A) as shown. From the figure, it can be observed that an elevation in the parameter Nb improves the thermal characteristics $\theta(\eta)$ of the working fluid temperature distribution, as seen in Fig. 6(A). This acceleration produces in the temperature due to the enlarging values of the Brownian motion parameter temperature $\theta(\eta)$ and concentration $\psi(\eta)$ for the $TiO_2 + CMC - water$ and $Fe_3O_4 + CMC - water$ nanofluid that reveals that erratic speed produces in the molecules suspended TiO_2 nanoparticles and Fe_3O_4 nanoparticles in water. The temperature gradient increases due to the rise in Nb, which is responsible for the speed-up of the zigzag motion of molecules within the fluid, due to which the temperature gets high. Similarly, the nanoparticle concentration profile $\psi(\eta)$ for the growing values of Nb is highlighted in Fig. 6(B). The plot of the high importance of Nb versus concertation profiles shows a decrement behavior. It is physically correct. This decrement in the concertation of the nanoparticles in both the cases $TiO_2 + CMC - water$ and $Fe_3O_4 + CMC - water$ nanofluid is due to the reason that increasing Nb there a chance of repetition interaction among the nanoparticles TiO_2 and Fe_3O_4 Consequently, the gap between the nanoparticles is reduced; hence, the concentration distribution decreases, as shown in Fig. 6(B).

4.6. Impact of Prandtl number

The impact of Pr versus temperature $\theta(\eta)$ for the $TiO_2 + CMC - water$ and $Fe_3O_4 + CMC - water$ nanofluid is highlighted in Fig. 7. The temperature curve for various values of Pr the parameter is highlighted in Fig. 7 as shown. From the figure, the high importance of Pr have shown a significant decrease in the thermal boundary physically. It is correct. This decrease in the temperature for higher values of Pr is because it controls the relative thickness of the thermal boundary layers, due to which the temperature of the fluid over s rotating disk declines for the higher values of Pr.

4.7. Impact of Schmidt number Sc

The impact of Sc on the concertation profile of the fluid is portrayed in Fig. 8. From the plot, it can be observed that higher values of the Sc will decline the concentration profile in the boundary layer region in both cases for the $TiO_2 + CMC - water$ and $Fe_3O_4 + CMC - water$ based nanofluid flow over a rotating disk as shown in the figure.
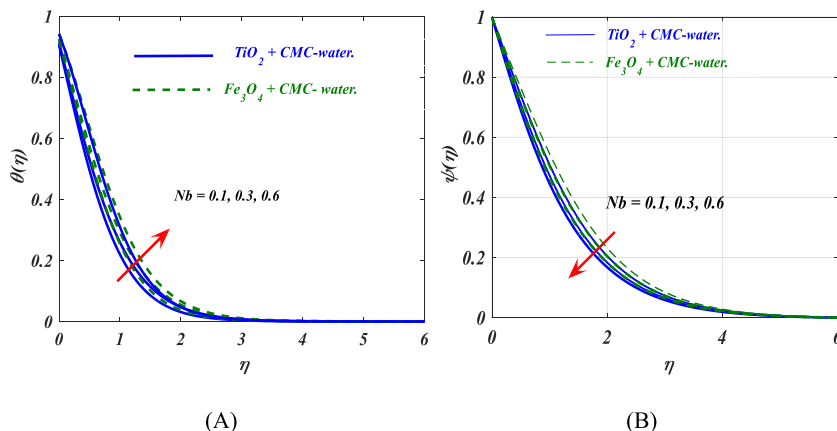
Fig. 6. Consequence of Nb on $(A)\theta(\eta)(B)\psi(\eta)$.
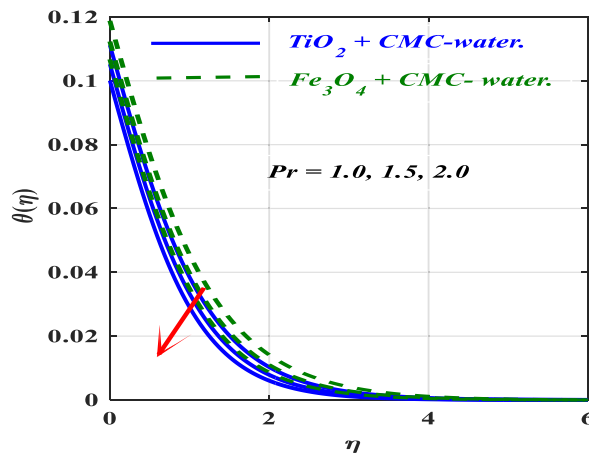
Fig. 7. Consequence of Pr on $\theta(\eta)$.

4.8. The impact of skin friction C_{fx}, Nusselt number Nu_x and Sherwood number Sh_x

The Skin Friction versus β against various values of Fr is portrayed in Fig. 9. The Nusselt number Nu versus Nt against escalating values of Nb is highlighted in Fig. 10. The Sherwood number Sh versus Nt against enhancing values of Sc is presented in Fig. 11. From the figure, it can be observed that the C_f, Nu and Sh are highlighted for water water base fluid containing TiO_2 and Fe_3O_4 nanoparticles and the fluid flow is considered over a stretching rotating disk. From Fig. 9 an increasing behavior is noticed in the C_f with escalating values of Fr. Similarly, the variation of Nu and Sh is portrayed in Figs. 10 and 11 which shows that the higher importance of the Nb and Sc the corresponding Nu and Sh get higher in both the cases $TiO_2 + CMC - water$ and $Fe_3O_4 + CMC - water$ based nanofluid flow over a rotating disk as shown in Figures.

4.9. Consequence of Fr on the contour line and streamline pattern

From Fig. 12(A) and (B), it can be observed that Fr plays a vital role in the dynamics of the hybrid nanofluid flow over a stretching rotating disk. The escalating values Fr of the streamlines get lower, as shown in the figure, which shows that Fr controls the fluid flow. The same behavior was noticed during the graphical analysis of Fr in Section 4.1 for the axial and radial velocity shown in Fig. 2(A) and (B), respectively. Figs. 13 and 14 exhibit the streamline for the numerous values of Fr.

5. Validation of the results

In addition to this, the comparison has also been performed in Table 2 with the previous literature that has been done by Ali et al.
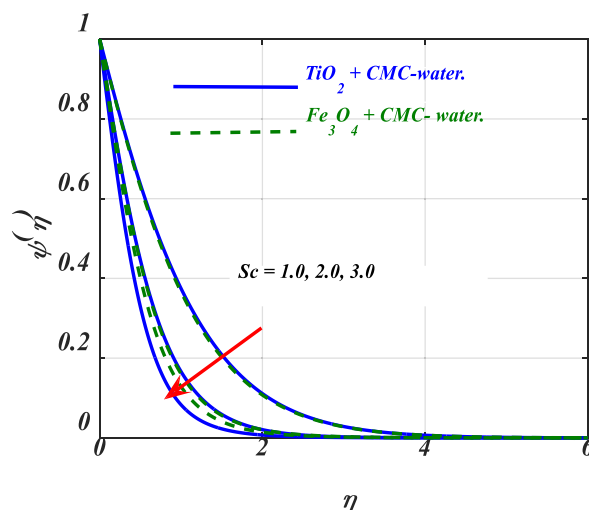
Fig. 8. Consequence of Sc on $\psi(\eta)$.
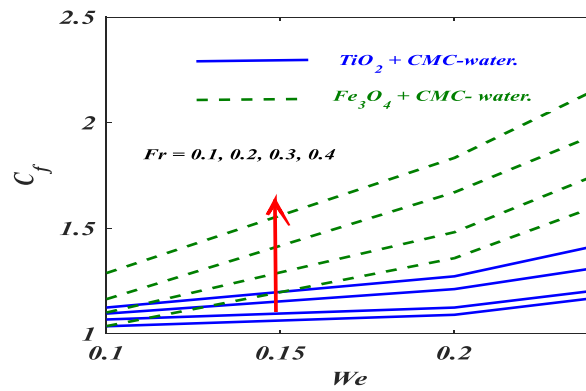
Fig. 9. Consequence of β and Fr on C_f.
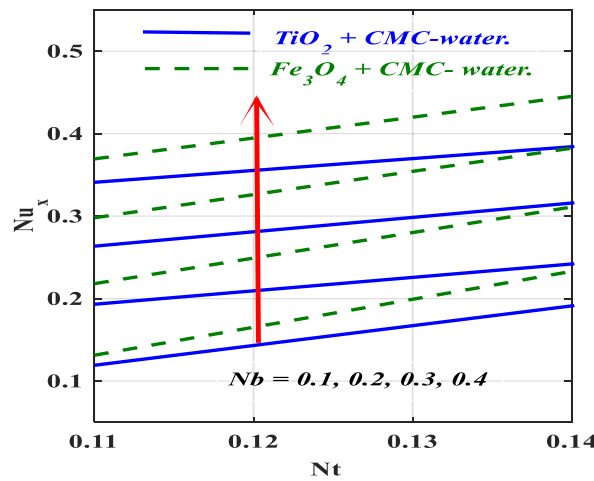
Fig. 10. Consequence of Nb and Nt on Nu.
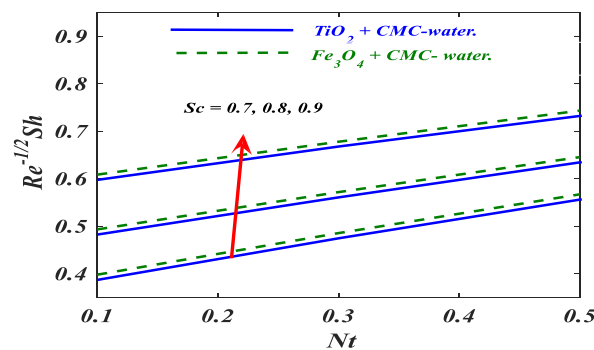
Fig. 11. Consequence of Nt and Sc on Sh.

[5] for $-\theta'(0)$ as a particular stance for our current study.

6. Table discussion

The information about the Skin Friction C_f, Nusselt Number Nu and Sherwood number Sh for $TiO_2 + CMC - water$ and $Fe_3O_4 + CMC - water$ based nanofluid flow over a rotating disk as shown in Tables 3–5. The impact of Fr results in the enhancement of the force friction in the case of $TiO_2 + CMC - water$ and $Fe_3O_4 + CMC - water$ as seen in Table 4. The heat and mass flux impact is tabulated in Table 5. The Sc, Nb, and Nt enhance the heat flux with an evident augmentation in mass flux.
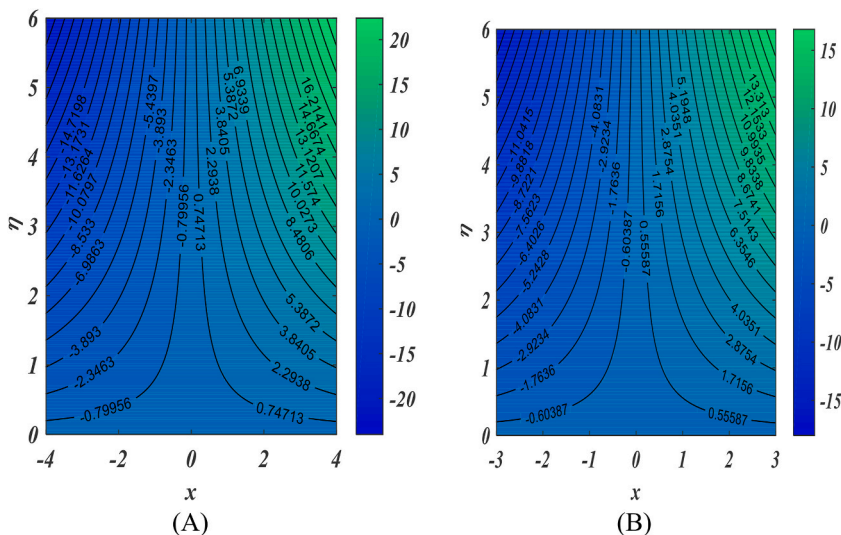
Fig. 12. Consequence of contour plot (A) $Fr = 0.0$ (b) $Fr = 0.3$.
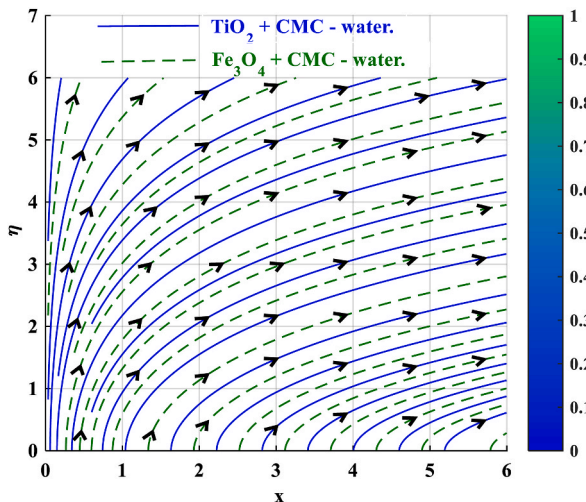
Fig. 13. Consequence of $Fr = 0.0$ on the streamline.

7. Concluding remarks

This research discussed the proposed model of Darcy Forchheimers flow of magnetite-CMC-water nanofluidover a rotating stretchable disk and the fluid contained $TiO_2 + CMC-$ water base and $Fe_3O_4 + CMC-$ water nanofluid. The stretchable rotating disk with heat and mass transfer disturbs the fluid.

During the present analysis, we get the following concluding remarks.

- The growing values Fr decline the axial velocity $F(\eta)$ and radial velocity $G(\eta)$ while increasing the azimuthal velocity $H(\eta)$ and temperature $\theta(\eta)$.
- The growing values of rotational parameter β accelerate the axial velocity $F(\eta)$ and radial velocity $G(\eta)$ while reducing the azimuthal velocity $H(\eta)$.
- The escalating values φ slow down the axial velocity $F(\eta)$ and radial velocity $G(\eta)$ while speeding up the azimuthal velocity $H(\eta)$ and temperature $\theta(\eta)$.
- The increase in the Nt result is an increase in both the thermal $\theta(\eta)$ and concentration $\psi(\eta)$ distribution.
- The higher values Nb increase the temperature $\theta(\eta)$ while declining the concentration $\psi(\eta)$ distribution.
- The growing values of Pr control thermal $\theta(\eta)$ profile.
- The increase in the Schmidt number declines concentration $\psi(\eta)$ distribution.
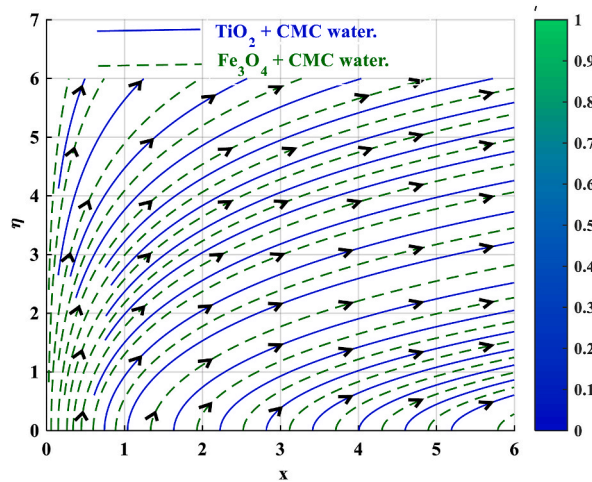
Fig. 14. Consequence of $Fr = 0.3$ on the streamline.

Table 2
Numerical comparison of Nusselt number for the various values of Pr.

Pr	Ali et al. [5]	Current outcomes
0.7	0.4560	0.4539
2.0	0.9113	0.9113
7.0	1.8954	1.8954
20	3.3539	3.3539

Table 3
The values of skin-friction co-efficient $C_f Re^{\frac{1}{2}}$ for different values of fluid parameters.

ω	β	M	φ	$C_f Re^{\frac{1}{2}}$	
				$TiO_2\ CMC-water$	$Fe_3O_4 + CMC-water$
0.5	0.1	1.0	0.01	1.7002	1.6901
1.0	0.1	1.0	0.01	2.2551	2.2441
1.5	0.1	1.0	0.01	2.9998	2.9887
1.5	0	1.0	0.01	3.0031	3.0016
1.5	0.2	1.0	0.01	2.9997	2.9884
1.5	0.3	1.0	0.01	2.2987	2.2876
1.5	0.3	0.5	0.01	2.7727	2.7617
1.5	0.3	1.5	0.01	3.2184	3.2072
1.5	0.3	2.5	0.01	3.6217	3.6109
1.5	0.3	2.5	0.02	3.7312	3.7202
1.5	0.3	2.5	0.03	3.8430	3.8321
1.5	0.3	2.5	0.04	3.9572	3.9461

- The C_{fx} get higher with the growing values of Fr verses β.
- The Nu_x increases with the elevated values of Nb versus Nt.
- The Sh_x get higher for the elevated values of Sc versus Nt.

Future direction

Our study was carried out on the Darcy-Forchheimer by considering CMC-water with two nanoparticles rotating using the Buongiorno model over a rotating disk. Mixed convective and MHD, multiple slip effect, and general fluids models may be included in future work if time and resources permit.

Table 4

The values of local Nusselt number $Nu\,Re^{-\frac{1}{2}}$ for different values of fluid parameters.

φ	Pr	Nt	Nb	$NuRe^{-\frac{1}{2}}$	
				$TiO_2\,CMC-water$	$Fe_3O_4+CMC-water$
0.01	6.7	0.4	0.4	0.4255	0.4145
0.01				0.4274	0.4164
0.01				0.4281	0.4172
0.01				0.4290	0.4169
0.01	6.7	0.4	0.4	0.4301	0.4291
0.01				0.4312	0.4201
0.02				0.4409	0.4399
0.03	6.7			0.4608	0.4597
0.04				0.4693	0.4582
0.04	5			0.4480	0.4368
0.04	6			0.4562	0.4451
0.04	7			0.4626	0.4515
0.04	7	0.2		0.4634	0.4523
0.04	7	0.5		0.4622	0.4512
0.04	7	0.8		0.4610	0.4500

Table 5

The values of local Nusselt number $Sh\,Re^{-\frac{1}{2}}$ for different values of fluid parameters.

Sc	Nt	Nb	$ShRe^{-\frac{1}{2}}$	
			$TiO_2\,CMC-water$	$Fe_3O_4+CMC-water$
0.7	0.4	0.4	0.6084	0.5973
0.8			0.6777	0.6676
0.9			0.7433	0.7321
0.7	0.5		0.4930	0.4821
0.8		0.4	0.5716	0.5605
0.9			0.6454	0.6343
0.7	0.6	0.5	0.3976	0.3866
0.8			0.4853	0.4743
0.9			0.5670	0.5559
0.7	0.7	0.6	0.3197	0.3086
0.8			0.4160	0.4049
0.9			0.5053	0.4942

Author contribution statement

Farhan Ali, Anwar Saeed: Analyzed and interpreted the data; Wrote the paper.
Muhammad Arif, Muhammad Faizan: Conceived and designed the analysis.
Thidaporn Seangwattana: Analyzed and interpreted the data.
PoomKumam: Contributed analysis tools or data; Wrote the paper.
Ahmed M. Galal: Conceived and designed the analysis; Wrote the paper.

Data availability statement

Data will be made available on request.

Declaration of competing interest

The authors declare that they have no known competing financial interests or personal relationships that could have appeared to

influence the work reported in this paper.

Nomenclature

λ	Porosity parameter Dimensionless
Fr	Darcy-Forchheimer Dimensionless
B_i	Biot number Dimensionless
Nb	Brownian motion Dimensionless
Nt	Thermophoresis force Dimensionless
Pr	Prandtl number Dimensionless
K^*	Mean absorption Dimensionless
Sc	Schmidt number Dimensionless
F	Dimensionless axial velocity Dimensionless
G	Dimensionless radial velocity Dimensionless
H	Dimensionless azimuthal velocity Dimensionless
ϑ	Dimensionless temperature field Dimensionless
φ	Dimensionless concentration field Dimensionless
τ	The ratio of effective heat capacity Dimensionless
Cf	Skin friction coefficient Dimensionless
Nu_r	Nusselt number Dimensionless
Sh_r	Sherwood number Dimensionless
r, φ, z	Cylindrical Dimensionless
β	Rotation parameter Dimensionless
u, v, w	Component of velocity ms^{-1}
ω	Angular velocity s^{-1}
c_p	Specific heat $J(kg)^{-1}K^{-1}$
g	Acceleration due to gravity ms^{-2}
D_T	Thermophoretic diffusion coefficient m^2s^{-1}
D_B	Brownian diffusion coefficient m^2s^{-1}
T	The temperature of the fluid K
T_w	Wall temperature K
T_∞	Ambient temperature K
T_f	Surface heat K
$h(t)$	Coefficient of heat transfer $Wk^{-1}m^{-2}$

Hybrid nanofluid

μ_{hnf}	Dynamic viscosity of CMC-wtaer $kg(ms)^{-1}$
v_{hnf}	Kinematic viscosity of CMC-wtaer m^2s^{-1}
α_{hnf}	Thermal diffusivity of CMC-wtaer m^2s^{-1}
k_{hnf}	Thermal conductivity of CMC-wtaer $kgmK^{-1}s^{-3}$
ρ_{hnf}	Density of nanofluid of CMC-wtaer kgm^{-3}
$(C_p)_{hnf}$	The density of microorganism particles kgm^{-3}

nanofluid

μ_{nf}	Dynamic viscosity of CMC-wtaer $kg(ms)^{-1}$
v_{nf}	Kinematic viscosity of CMC-wtaer m^2s^{-1}
α_{nf}	Thermal diffusivity of CMC-wtaer m^2s^{-1}
k_{nf}	Thermal conductivity of CMC-wtaer $kgmK^{-1}s^{-3}$
ρ_{nf}	Density of nanofluid of CMC-wtaer kgm^{-3}
$(C_p)_{nf}$	The density of microorganism particles kgm^{-3}

References

[1] I.H. Mondal, Carboxymethyl Cellulose: Synthesis and Characterization, Nova Science Publishers, Hauppauge, NY, USA, 2019.

[2] A. Benchabane, K. Bekkour, Rheological properties of carboxymethyl cellulose (CMC) solutions, Colloid Polym. Sci. 286 (10) (2008) 1173–1180.

[3] A. Babazadeh, M. Tabibiazar, H. Hamishehkar, B. Shi, Zein-CMC-PEG multiple nanocolloidal systems as a novel approach for nutra-pharmaceutical applications, Adv. Pharmaceut. Bull. 9 (2) (2019) 262.

[4] E.J. Siqueira, M.C.B. Salon, M.N. Belgacem, E. Mauret, Carboxymethylcellulose (CMC) as a model compound of cellulose fibers and polyamideamineepichlorohydrin (PAE)–CMC interactions as a model of PAE–fibers interactions of PAE-based wet strength papers, J. Appl. Polym. Sci. 132 (26) (2015).

[5] F. Ali, K. Loganathan, S. Eswaramoorthi, K. Prabu, A. Zaib, Dinesh Kumar Chaudhary, Heat transfer analysis on carboxymethyl cellulose water-based cross hybrid nanofluid flow with entropy generation, J. Nanomater. (2022), e5252918, https://doi.org/10.1155/2022/5252918.

[6] F. Ali, T.A. Kumar, K. Loganathan, C.S. Reddy, A.A. Pasha, M.M. Rahman, K. Al-Farhany, Irreversibility analysis of cross fluid past a stretchable vertical sheet with mixture of carboxymethyl cellulose water based hybrid nanofluid, Alex. Eng. J. 64 (2023) 107–118.

[7] C.B. Hollabaugh, L.H. Burt, A.P. Walsh, Carboxymethylcellulose. Uses and applications, Ind. Eng. Chem. 37 (10) (1945) 943–947.

[8] I.H. Mondal, Carboxymethyl Cellulose, vol. II, Nova Science Publishers, 2019. Incorporated.

[9] E. Grządka, J. Matusiak, A. Bastrzyk, I. Polowczyk, CMC as a stabiliser of metal oxide suspensions, Cellulose 27 (4) (2020) 2225–2236.

[10] S.U. Choi, J.A. Eastman, Enhancing Thermal Conductivity of Fluids with Nanoparticles, Argonne National Lab, IL (United States), 1995.

[11] M.S. Sami, Ahmed, M. Sabyasachi, P. Sibanda, Impulsive nanofluid flow along a vertical stretching cone, Int. J. Heat Tech. 35 (4) (2017) 1005–1014.

[12] M.S. Sami, Ahmed, M. Sabyasachi, P. Sibanda, Double-diffusive convection in unsteady magneto-nanofluid flow, Adv. Nanotech. 21 (2018) 215–240.

[13] I.S. Oyelakin, P. Mondal, S. Mondal, T. R Mahapatra, P. Sibanda, Rheological analysis of suspended single-walled carbon nanotubes in a walters, B fluid Nanosci. Nanotechnol.-Asia 11 (6) (2021), e190820185096.

[14] S. Mondal, N.A.H. Haroun, S.K. Nandy, P. Sibanda, MHD boundary layer flow and heat transfer of Jeffrey nanofluid over an unsteady shrinking sheet with partial slip, J. Nanofluids 6 (2) (2017) 343–353.

[15] I.S. Oyelakin, P.C. Lalramneihmawii, S. Mondal, P. Sibanda, Analysis of double-diffusion convection on three-dimensional MHD stagnation point flow of a tangent hyperbolic Casson nanofluid, Int. J. Ambient Energy 43 (1) (2022) 1854–1865.

[16] G. Sicelo, P. Mondal, M. Sabyasachi, P. Sibanda, S.S. Motsa, Unsteady mixed convection in nanofluid flow through a porous medium with thermal radiation using the bivariate spectral quasilinearization method, J. Nanofluids 6 (2) (2017) 273–281.

[17] G. Sicelo, P. Mondal, M. Sabyasachi, P. Sibanda, S.S. Motsa, An unsteady magnetohydrodynamic jeffery nanofluid flow over a shrinking sheet with thermal radiation and convective boundary condition using spectral quasilinearisation method, J. Comput. Theor. Nanosci. 13 (2016) 7483–7492.

[18] Z.M. Mburu, M.K. Nayak, S. Mondal, P. Spinda, Impact of irreversibility ratio and entropy generation on three-dimensional Oldroyd-B fluid flow with relaxation-retardation viscous dissipation, Indian J. Phys. 96 (1) (2022) 151–167.

[19] A.H. Nageeb, Haroun, M. Sabyasachi, S. Mondal, P. Sibanda, Hydromagnetic nanofluids flow through a porous medium with thermal radiation, chemical reaction and viscous dissipation using the spectral relaxation method, Int. J. Comput. Methods 15 (1) (2018) 1–19.

[20] R. Ghosh, M. Titilayo, T.M. Agbaje, M. Sabyasachi, S. Mondal, S. Shaw, Bio-convective viscoelastic Casson nanofluid flow over a stretching sheet in the presence of induced magnetic field with Cattaneo-Christov double diffusion, Int. J. Biomath. (IJB) 15 (3) (2021), 2150099.

[21] F. Ali, A. Zaib, K. Loganathan, A. Saeed, T. Seangwattana, P. Kumam, A.M. Galal, Scrutinization of second law analysis and viscous dissipation on ReinerRivlinNanofluid with the effect of bioconvection over a stretching sheet, Heliyon (9) (2023), E13091.

[22] J. Buongiorno, Convective transport in nanofluids, J. Heat Tran. 128 (2006) 240.

[23] A. Abbasi, W. Farooq, E.S.M. Tag-ElDin, S.U. Khan, M.I. Khan, K. Guedri, S. Elattar, M. Waqas, A.M. Galal, Heat transport exploration for hybrid nanoparticle (Cu, Fe3O4)-based blood flow via tapered complex wavy curved channel with slip features, Micromachines 13 (2022) 1415, https://doi.org/10.3390/mi13091415.

[24] Y.M. Chu, M.I. Khan, T. Abbas, M.O. Sidi, K.A.M. Alharbi, U.F. Alqsair, S.U. Khan, M.R. Khan, M.Y. Malik, Radiative thermal analysis for four types of hybrid nanoparticles subject to non-uniform heat source: keller box numerical approach, Case Stud. Therm. Eng. 40 (2022), 102474.

[25] I. Ullah, Tasawar Hayat, Alsaedi Ahmed, S. Asghar, Dissipative flow of hybrid nanoliquid (H2O–aluminum alloy nanoparticles) with thermal radiation, Phys. Scripta 94 (2019), 125708, https://doi.org/10.1088/1402-4896/ab31d3.

[26] G. Sowmya, B.J. Gireesha, S. Sindhu, B.C. Prasannakumara, Investigation of Ti6Al4V and AA7075 alloy embedded nanofluid flow over longitudinal porous fin in the presence of internal heat generation and convective condition, Commun. Theor. Phys. 72 (2020), 025004, https://doi.org/10.1088/1572-9494/ab6904.

[27] H. Xu, Q. Sun, Generalized hybrid nanofluid model with the application of fully developed mixed convection flow in a vertical microchannel, Commun. Theor. Phys. 71 (2019) 903, https://doi.org/10.1088/0253-6102/71/8/903.

[28] L.A. Lund, Z. Omar, S. Dero, I. Khan, D. Baleanu, K.S. Nisar, Magnetized flow of Cu + Al2O3 + H2O hybrid nanofluid in porous medium: analysis of duality and stability, Symmetry 12 (9) (2020) 1513.

[29] W. Hassan, U. Farooq, R. Naseem, S. Hussain, M. Alghamdi, Impact of MHD radiative flow of hybrid nanofluid over a rotating disk, Case Stud. Therm. Eng. 26 (2021), 101015, https://doi.org/10.1016/j.csite.2021.101015.

[30] M.K. Nayak, MHD 3D flow and heat transfer analysis of nanofluid by shrinking surface inspired by thermal radiation and viscous dissipation, Int. J. Mech. Sci. 124–125 (2017) 185–193.

[31] M.S. Sadeghi, T. Tayebi, A.S. Dogonchi, M.K. Nayak, M. Waqas, Analysis of thermal behavior of magnetic buoyancy-driven flow in ferrofluid–filled wavy enclosure furnished with two circular cylinders, Int. Commun. Heat Mass Tran. 120 (2021), 104951, https://doi.org/10.1016/j.icheatmasstransfer.2020.104951.

[32] S. Shaw, S.S. Samantaray, A. Misra, M.K. Nayak, O.D. Makinde, Hydromagnetic flow and thermal interpretations of cross hybrid nanofluid influenced by linear, nonlinear and quadratic thermal radiations for any Prandtl number, Int. Commun. Heat Mass Tran. 130 (2022), 105816, https://doi.org/10.1016/j.icheatmasstransfer.2021.105816.

[33] M.K. Nayak, N. Karimi, A.J. Chamkha, A.S. Dogonchi, S. El-Sapa, A.M. Galal, Efficacy of diverse structures of wavy Baffles on heat transfer amplification of double-diffusive natural convection inside a C-shaped enclosure filled with hybrid nanofluid, Sustain. Energy Technol. Assessments 52 (2022), 102180, https://doi.org/10.1016/j.seta.2022.102180.

[34] M.K. Sarangi, D.N. Thatoi, M.K. Nayak, J. Prakash, K. Ramesh, M. Azam, Rotational flow and thermal behavior of ternary hybrid nanomaterials at small and high Prandtl numbers, Int. Commun. Heat Mass Tran. 138 (2022), 106337, https://doi.org/10.1016/j.icheatmasstransfer.2022.106337.

[35] H. Rout, S.S. Mohapatra, S. Shaw, T. Muhammad, M.K. Nayak, O.D. Makinde, Entropy optimization for Darcy–Forchheimer electro-magneto-hydrodynamic slip flow of ferronanofluid due to stretching/shrinking rotating disk, Waves Random Complex Media (2021), https://doi.org/10.1080/17455030.2021.1927238.

[36] A.K. Hakeem, M.K. Nayak, O. D Makinde, Effect of exponentially variable viscosity and permeability on Blasius flow of Carreaunano fluid over an electromagnetic plate through a porous medium, J. App. Comp. Mech. 5 (2) (2019) 390–401.

[37] Kushal Sharma, S. Kumar, N. Vijay, Insight into the motion of water-copper nanoparticles over a rotating disk moving upward/downward with viscous dissipation, Int. J. Mod. Phys. B 36 (29) (2022), 2250210, https://doi.org/10.1142/S0217979222502101.

[38] Sanjay Kumar, K. Sharma, Darcy-Forchheimer fluid flow over stretchable rotating disk moving upward/downward with heat source/sink, special topics & reviews in porous media, Int. J. 13 (2022) 4, https://doi.org/10.1615/SpecialTopicsRevPorousMedia.2022043951.

[39] Sanjay Kumar, K. Sharma, Entropy optimized radiative heat transfer of hybrid nanofluid over vertical moving rotating disk with partial slip, Chin. J. Phys. 77 (2022) 861–873, https://doi.org/10.1016/j.cjph.2022.03.006.

[40] D. Ziental, C. Goslinska, B. Mlynarczyk, D.T. G Sobotta, A. Stanisz, B. Goslinski, T. Sobotta, Titanium dioxide nanoparticles: prospects and applications in medicine, Nanomaterials 10 (2) (2020) 387.

[41] M.A. Behnam, F. Emami, F.Z. Sobhani, A.R. Dehghanian, The application of titanium dioxide (TiO2) nanoparticles in the photo-thermal therapy of melanoma cancer model, Ir. J. bas. Med. Sci. 21 (11) (2018) 1133.

[42] H. Shi, R. Magaye, V. Castranova, J. Zhao, Titanium dioxide nanoparticles: a review of current toxicological data, Part. Fibre Toxicol. 10 (1) (2013) 1–33.

[43] P.L. Sanches, L.R. Geaquinto, D.O. Cruz, R. Schuck, D.C. Lorencini, M. Granjeiro, J.M. Ribeiro, Toxicity evaluation of TiO2 nanoparticles on the 3D skin model: a systematic review, Front. Bioeng. Biotechnol. 8 (2020) 575.

[44] V.K. Sharma, Aggregation and toxicity of titanium dioxide nanoparticles in aquatic environment—a review, J. Env. Sci. Health Part A 44 (14) (2009) 1485–1495.

[45] S. Yuan, W. Chen, S. Hu, Fabrication of TiO2 nanoparticles/surfactant polymer complex film on glassy carbon electrode and its application to sensing trace dopamine, Mater. Sci. Eng. C 25 (4) (2005) 479–485.

[46] T. Von Kármán, Uber laminare und turbulenteReibung, Z. Angew. Math. Mech. 1 (1921) 233–252.

[47] E.R. Benton, On the flow due to a rotating disk, J. Fluid Mech. 24 (4) (1966) 781–800.

[48] A.G. Emslie, F.T. Bonner, L.G. Peck, Flow of a viscous liquid on a rotating disk, J. Appl. Phys. 29 (5) (1958) 858–862.

[49] E.C. Cobb, O.A. Saunders, Heat transfer from a rotating disk, Proc. Royal Society London. Ser. A. Proc. Math. Phys. 236 (1206) (1956) 343–351.

[50] Z. Wang, W. Wang, S. Liu, N. Yang, G. Zhao, Coupling rotating disk electrodes and surface-enhanced Raman spectroscopy for in situ electrochemistry studies, Electrochem. Commun. 124 (2021) 106928.

[51] O.A. Bég, M.N.U. Kabir, M.J. Izani, A. Md Ismail, Y.M. Alginahi, Numerical investigation of Von Karman swirling bioconvectivenanofluid transport from a rotating disk in a porous medium with Stefan blowing and anisotropic slip effects, Proc. IME C J. Mech. Eng. Sci. 235 (19) (2021) 3933–3951.

[52] N. Gregory, J.T. Stuart, W.S. Walker, On the stability of three-dimensional boundary layers with application to the flow due to a rotating disk, Philosophical Trans. Royal Society London. Ser. A, Proc. Math. Phys. 248 (943) (1955) 155–199.

[53] A. Mushtaq, M. Mustafa, Computations for nanofluid flow near a stretchable rotating disk with axial magnetic field and convective conditions, Results Phys. 7 (2017) 3137–3144.

[54] J.A. Khan, M. Mustafa, T. Hayat, A. Alsaedi, A revised model to study the MHD nanofluid flow and heat transfer due to rotating disk: numerical solutions, Neural Comput. Appl. 30 (3) (2018) 957–964.

[55] M. Asma, W.A.M. Othman, T. Muhammad, Numerical study for Darcy–Forchheimer flow of nanofluid due to a rotating disk with binary chemical reaction and Arrhenius activation energy, Mathematics 7 (10) (2019) 921.

[56] K.U. Rehman, M.Y. Malik, M. Zahri, M. Tahir, Numerical analysis of MHD CassonNavier's slip nanofluid flow yield by rigid rotating disk, Res. Pys. 8 (2018) 744–751.

[57] M.A. Sadiq, F. Haider, T. Hayat, A. Alsaedi, Partial slip in Darcy-Forchheimer carbon nanotubes flow by rotating disk, Int. Commun. Heat Mass Tran. 116 (2020) 104641.

[58] M.Z. Ullah, S. Capizzano, S. Baleanu, A numerical simulation for Darcy-Forchheimer flow of nanofluid by a rotating disk with partial slip effects, Front. Physiol. 7 (2020) 219.

[59] S.M.R.S. Naqvi, T. Muhammad, H.M. Kim, T. Mahmood, A. Saeed, B. Khan, Numerical treatment for Darcy–Forchheimer flow of nanofluid due to a rotating disk with slip effects, Can. J. Phys. 97 (8) (2019) 856–863.

[60] Asifa Tassaddiq, S. Khan, M. Bilal, T. Gul, S. Mukhtar, Z. Shah, E. Bonyah, Heat and mass transfer together with hybrid nanofluid flow over a rotating disk, AIP Adv. 10 (5) (2020), 055317, https://doi.org/10.1063/5.0010181.

[61] Sabu, A.S., Ali, F., Reddy, C.S., Areekara, S., Mathew, A.: Insight on the dynamics of hydromagnetic stagnation-point flow of magnetite-water nanofluid due to a rotating stretchable disk: a two-phase modified Buongiorno modeling and simulation. Z. Angew. Math. Mech. e202100520.